Submitted to Optics Communications
24.11.99
1946

Analysis Method for Apodised Grating Structures

I.A. Goncharenko* and M. N. Zervas**

*Institute of Electronics, National Academy of Sciences of Belarus
22 Lagoiski Trakt, Minsk, 220090, Belarus
** Optoelectronics Research Centre, University of Southampton
Southampton SO17 1BJ, UK

Abstract

A modified method of lines (MoL) technique is presented for calculating the reflection characteristics of apodised fibre gratings. To demonstrate the technique, reflection spectra of fibre gratings with triangular and diamond apodisation profiles have been calculated showing significant side-lobe suppression. MoL can accurately calculate not only average power but also field and phase distribution across reflected waves. It has been shown that the phase of the reflected light is maximally affected at the edge of the grating stop-band.

PACS: 4279Dj; 7820Bh
Keywords: Fibre gratings; Apodisation; Method of Lines

** Corresponding author : M.N.Zervas. Tel.: +44 1703 593147; Fax: +44 1703 593149; e-mail: mnz@orc.soton.ac.uk

It is now well established that fibre Bragg gratings (FBGs) will play an important role in the implementation of a number of high performance devices used to provide optical feedback, wavelength control, filtering, pulse compression and dispersion compensation [1,2]. In addition to uniform periodic structures, specially designed FBGs with modified characteristics, such as chirped and apodised gratings have also been extensively studied and successfully demonstrated. Chirped fibre gratings have a continuously varying local period and, therefore, show wide reflection bandwidths and large in-band dispersion [3]. Their characteristics are easily controllable and can be used for efficient dispersion compensation in fibre communication links [4]. Apodised periodic fibre gratings, on the other hand, have variable coupling strength along their length and show reflection spectra with reduced sidelobes [5]. The time delay and reflection characteristics of linearly chirped FBGs are also shown to improve considerably when proper apodisation profiles are applied [6].

Among the most commonly used techniques for the analysis of FBGs are the coupled-mode theory (CMT) [7-8] and the transfer-matrix method (TMM) [9-10]. CMT is a powerful mathematical formulation that describes power transfer and evolution in a number of different continuous optical structures. It is based on the "slow-amplitude approximation", and it is, therefore, applicable to situations that the optical powers change slightly over an optical wavelength. However, CMT is proved to be very accurate in most practical cases. TMM, on the other hand, is a much more general computational technique and can accurately describe the power evolution in much more complex optical structures involving discontinuities and spatial-phase shifts. In general, TMM is an exact method. Another powerful technique widely used for the analysis of general periodic structures is formulated in terms of the Floquet theorem and involves Bloch modes [11-12].

Recently, another method has been proposed for the analysis of periodic uniform gratings based on the method of lines (MoL) [13-14]. MoL is a special finite-difference method that enables the analysis of wave propagation in multi-layer waveguides and fibre structures. This method uses a semi-analytical approach, which yields accurate results with less computational effort compared to other techniques. In MoL the mode coupling and scattering losses are automatically taken into account. We have already applied successfully this method to calculate the reflection and transmission characteristics of uniform periodic fibre gratings [15] and analyze nonlinear fibre Bragg gratings [16].

In this work we extend the basic method of lines to analyse apodized fibre grating structures. The first step of the algorithm is analogous to [15,16]. We start with the vector wave equation for the vector potential $\mathbf{\Pi}$, namely [17]:

$$\begin{aligned} &\nabla^2\mathbf{\Pi} - \varepsilon^{-1}(\nabla\varepsilon)\nabla\cdot\mathbf{\Pi} + \varepsilon\mathbf{\Pi} = \mathbf{0} \\ &\eta_0\mathbf{H} = j\nabla\times\mathbf{\Pi} \\ &\mathbf{E} = \varepsilon^{-1}\nabla\times\nabla\times\mathbf{\Pi}. \end{aligned} \tag{1}$$

where, in general, $\varepsilon = n^2$ is the dielectric permittivity ($n = n_{co}, n_{cl}$ are the refractive indices in the fibre core and cladding, respectively). The dielectric permittivity is considered to be a general function of the cylindrical coordinates (r, φ, z).

To implement the method, the apodised fibre grating structure is divided into homogeneous sections with different propagation constants (see Figure 1(a)). In each section the dielectric permittivity is only a function of the transverse coordinates, i.e. $\varepsilon = \varepsilon(r,\varphi)$. In this case only the two transverse components of $\mathbf{\Pi}$ need to be considered. In our calculations, we assume that the fibre is isotropic and therefore $\varepsilon(\varphi)$ is constant. Thus, the φ-dependence of the vector potentials can be described by:

$$\begin{aligned} \Pi_r(r,\varphi,z) &= \Pi_r(r,z)\cos(m\varphi) \\ \Pi_\varphi(r,\varphi,z) &= \Pi_\varphi(r,z)\sin(m\varphi) \end{aligned}$$

and their derivatives with respect to coordinate φ can be determined analytically. After some mathematical manipulations, wave equation (1) can be written in cylindrical coordinates as [18]

$$\begin{aligned} &\bar{r}_n\varepsilon\frac{\partial}{\partial\bar{r}}\left(\bar{r}_n^{-1}\varepsilon^{-1}\frac{\partial}{\partial\bar{r}}\left(\bar{r}_n\Pi_r\right)\right) + \left(\varepsilon - \frac{\bar{m}^2}{\bar{r}_n^2}\right)\left(\bar{r}_n\Pi_r\right) + \frac{\partial^2\left(\bar{r}_n\Pi_r\right)}{\partial\bar{z}^2} + \bar{r}_n\varepsilon\bar{m}\frac{\partial}{\partial\bar{r}}\left(\varepsilon^{-1}\bar{r}_n^{-2}\left(\bar{r}_n\Pi_\varphi\right)\right) - \\ &- \frac{\bar{m}}{\bar{r}_n}\frac{\partial}{\partial\bar{r}}\left(\bar{r}_n\Pi_\varphi\right) = 0 \\ &\bar{r}_n\frac{\partial}{\partial\bar{r}}\left(\bar{r}_n^{-1}\frac{\partial}{\partial\bar{r}}\left(\bar{r}_n\Pi_\varphi\right)\right) + \left(\varepsilon - \frac{\bar{m}^2}{\bar{r}_n^2}\right)\left(\bar{r}_n\Pi_\varphi\right) + \frac{\partial^2\left(\bar{r}_n\Pi_\varphi\right)}{\partial\bar{z}^2} + \bar{r}_n\bar{m}\frac{\partial}{\partial\bar{r}}\left(\bar{r}_n^{-2}\left(\bar{r}_n\Pi_r\right)\right) - \\ &- \frac{\bar{m}}{\bar{r}_n}\frac{\partial}{\partial\bar{r}}\left(\bar{r}_n\Pi_r\right) = 0 \end{aligned} \tag{2}$$

where the coordinates and dimensions are normalized with respect to free-space wave number k_0 . Namely, $\bar{z} = k_0 z$, $\bar{r} = k_0 r$, $\bar{r}_n = \bar{r}/\bar{R}_{co,}$ $\bar{\varphi} = \bar{R}_{co}\varphi$, $\bar{m} = m/\bar{R}_{co}$ and $\bar{R}_{co} = R_{co}k_0$, where R_{co} is the fibre core radius.

Expression (2) is a system of two coupled partial differential equations. Following the MoL, coupled partial differential equations have to be discretized with respect to the r

coordinate using finite differences. This results in a system of ordinary differential equations, which can be solved analytically. In this case, all potentials and dielectric permittivities, as well as, the radial coordinate r have to be discretized [18]. The discretisation algorithm for apodised fibre gratings is the exactly same with the one used for the uniform gratings [15]. The algorithm has been detailed in Ref. [15] and will not be repeated here.

In a similar manner to the well-established impedance-matching technique [19], we represent each grating section with its characteristic wave impedance $\overline{Z}_0$ [15]. The wave impedance of the homogeneous section at the end of the fibre grating (where only forward propagating modes exist) is the load wave impedance at the output of the fibre grating, i.e. $\overline{\mathbf{Z}}_0^{out} = \overline{\mathbf{Z}}_{out}$. The technique involves the successive transfer of the load output wave impedance to the input of the grating and, in that way, determines the input impedance of the entire grating structure. Because in an apodized structure, the refractive index modulation varies continuously along the grating length, the impedance matching should be applied on each grating layer. However, since fibre gratings can be long involving a large number of periods, such approach would require extremely long computation time. The apodisation profiles considered in this study are shown schematically in Figure 1(b)-(d).

To decrease the numerical effort, we propose the same iteration algorithm, which was introduced and applied successfully in the analysis of nonlinear fibre gratings [16]. The technique involves the division of the apodised grating in a number of different sections. Each section is considered to be several-grating-period long and uniform. Therefore, the core refractive index change $\Delta n_{co} = (n_{co1} - n_{co2})/n_{co1}$ along each section is constant. Δn_{co}, however, varies from section to section. The derivation of the wave impedance in each uniform grating section can be derived by Floquet's theorem [15,20]. Following the algorithm presented in [15,16], we progressively transfer the impedance $\overline{\mathbf{Z}}_{out}$ from the far end of the entire grating, through the successive grating sections, to the front end of the grating. In such a way, the wave impedance at the input of the entire fibre grating structure is obtained. Using the initial conditions, the electric and magnetic fields of the incident ($\mathbf{E}_{in}^{f}$ and $\mathbf{H}_{in}^{f}$) and reflected ($\mathbf{E}_{in}^{b}$ and $\mathbf{H}_{in}^{b}$) waves at the input of the fibre grating can be determined. Following a similar procedure in the reverse direction, the input values of the electric and magnetic fields can be used to determine the field distribution at any point along the grating. Full knowledge of the electromagnetic field components along the fibre grating can provide useful information about field and phase distributions, as well as, calculation of reflection and transmission

coefficients. For instance, the grating reflection coefficient is determined as the amplitude ratio between backward- and forward-propagating electric fields at the grating input end.

The calculation accuracy depends on the number of grating sub-sections (N_{sect}). In order to check the accuracy and rate of convergence, for a given wavelength, the number of grating sections is successively increased by a factor of 2 until the difference in calculated reflectivities is below a certain limit. If n_{it} denotes the number of iterations, the corresponding number of sub-sections is $N_{sect} = 2^{n_{it}}$. Each section is comprised of N/N_{sect} number of periods (N is the total number of periods). Figure 2 shows the reflectivity accuracy (in %) as a function of the number of iterations n_{it}, for two apodised grating with different lengths $L_{gr} = N \cdot \Lambda$, where Λ is the length of grating periods. In contrast with nonlinear grating analysis [16], for a given N_{sect}, the accuracy and convergence rate is the same for all incident wavelengths. It is shown that a 0.1% accuracy of the reflectivity for the apodized fibre grating (triangular apodisation - see Fig.3(c)) is achieved with $N_{sect} = 2^5 = 32$ and $N_{sect} = 2^7 = 128$ for grating length of $L_{gr} = 2048 \cdot \Lambda$ (curve 1) and $L_{gr} = 4096 \cdot \Lambda$ (curve 2), respectively. In addition to grating length, the number of sections required for 0.1% reflectivity convergence will depend on the exact apodisation profile.

In all calculations reported in this paper, the fibre core radius is R_{co}=2μm, the core refractive index is n_{co}=1.45 and the refractive index step is Δ=0.005. The grating period is Λ=0.528μm and the maximum relative core index difference Δn_{co} at the grating centre is 0.001 unless otherwise stated.

Figure 3 shows the reflectivity spectra of apodised gratings with N = 4096 obtained with the modified MoL. Curves 1, 2 and 3 correspond to square, triangular and diamond apodisation profiles, respectively (see Fig. 1(b)-(d)). In each case, the corresponding maximum Δn_{co} is adjusted to result in approximately equal maximum reflectivity. As expected, it is shown that grating apodisation results in significant decrease of the reflectivity sidelobes. The main Bragg wavelength of the apodised gratings is shifted to longer wavelengths because of the increased average effective index over the grating area. The corresponding maximum Δn_{co} in the three cases was 0.0005 for curve 1 and 0.0010 for curves 2 and 3.

As already mentioned, one of the unique features of the MoL is that it takes accurately into account the propagating field exact transverse profile. Therefore it can be used to calculate the transverse field and phase distribution at any point along the grating for any

electric or magnetic field components. Figures 4(a) and (b) show the modulus and phase distribution of the electric field tangential components as a function of the normalised fibre radius of the forward- and backward-propagating fields at the grating input, for wavelengths corresponding maximum (λ_1), 3dB (λ_2) and minimum (λ_3) reflectivity. It is shown that the backward-propagating (reflected) field becomes progressively smaller and its phase transverse distribution less uniform as the wavelength is approaching the band-gap edge. The phase of the incident wave is constant across the entire field distribution. At the Bragg (λ_1) and 3dB (λ_2) wavelengths, the phase distribution is almost constant due to minimum penetration and small interaction with the periodic medium. There is only a fixed phase delay due to different degrees of penetration. At the band-gap edge, however, there is significant phase non-uniformity observed. This is due to the multiple trapping and effective time delay increase associated with the band-gap edge. The phase in the core region is retarded the most because of the higher index of this region. To the best of our knowledge, such an effect is reported for the first time. The unapodised grating has been chosen for this demonstration since the three aforementioned wavelengths are better defined. Similar effects are observed with the apodised gratings.

In conclusion, we have modified the MoL technique to calculate the reflection characteristics of apodised fibre gratings. The method involves proper segmentation and step-wise approximation of the actual continuously-apodised gratings. Application of Floquet's theorem on each uniform sub-section results in a fast converging algorithm capable of calculating long gratings. To demonstrate the technique, we have calculated reflection spectra of fibre gratings with triangular and diamond apodisation profiles, showing significant side-lobe suppression. MoL takes accurately into account the actual field and phase distributions of the interacting modes and is, therefore, uniquely poised to calculate not only average power but also field and phase distribution across reflected waves. It has been shown that the phase of the reflected light is maximally affected at the edge of the grating stop-band.

References:

1. J.-L. Archambault, S. G. Grubb, "Fiber gratings in lasers and amplifiers", *J. Lightwave Technol.* , vol. **15**, pp. 1378-1390 (1997).
2. C. R. Giles, "Lightwave applications of fiber gratings", *J. Lightwave Technol.*, vol. **15**, pp. 1391-1404 (1997).
3. K. O. Hill, F. Bilodeau, B. Malo, T. Kitagawa, S. Theriault, D. C. Johnson, J. Albert, "Chirped in-fiber Bragg gratings for compensation of optical-fiber dispersion", *Opt. Lett.*, vol. **19**, pp.1314-1316 (1994).
4. S. Barcelos, M. N. Zervas, R. I. Laming, "Characteristics of chirped fiber gratings for dispersion compensation, *Optic. Fiber Technol.*, vol. **2**, pp. 213-215 (1996).
5. P. S. Cross and H. Kolgenik, "Sidelobe suppression in corrugated waveguide filters", *Opt. Lett.*, vol. **1**, pp. 43-45 (1977).
6. K. Ennser, M. N. Zervas and R. I. Laming, "Optimisation of apodised linearly-chirped fibre gratings for optical communications", *IEEE J. Quantum Electron.*, vol. **34**, no. 5, pp. 770-778 (1998).
7. H. Kogelnik, "Theory of optical waveguides", in *Guided-Wave Optoelectronics*, T. Tamir (ed), Springer-Verlag (1988), Chapter 2.
8. A. Yariv and M. Nakamura, "Periodic structures for integrated optics", *IEEE J. Quant. Electron.*, vol. 13, no. 4, pp. 233-253 (1977).
9. P. Yeh, A. Yariv and C-S. Hong, "Electromagnetic propagation in periodic stratified media. I. General theory", *J. Opt. Soc. Am.*, vol. **67**, no. 4, pp. 423-438 (1977).
10. M. Yamada and K. Sakuda, "Analysis of almost-periodic distributed feedback slab waveguides via a fundamental matrix approach", *Appl. Opt.*, vol. **26**, no. 16, pp. 3474-3478 (1987).
11. R. E. Collin, "*Field Theory of Guided Waves*", 2nd edition, IEEE Press, 1991, Chapter 9.
12. A. Yariv and P. Yeh, "*Optical Waves in Crystals*", J. Wiley & Sons, 1984, Chapter 6.
13. R. Pregla, W. Pascher, "The method of lines", in *Numerical Techniques for Microwave and Millimetre Wave Passive Structures.* Ed. T. Itoh (N. York, J. Wiley & Sons, 1989), pp 381-446.

14. R. Pregla, "The method of lines as generalized transmission line technique for the analysis of multilayered structures", *AEÜ (Intern. J. Electron. Commun.),* vol. **50**, pp. 293-300 (1996).

15. I. A. Goncharenko, S. F. Helfert, R. Pregla, "General analysis of fibre grating structures", *J. Opt. A: Pure and Applied Optics*, vol, **1**, pp. 25-31 (1999).

16. I. A. Goncharenko, S. F. Helfert, R. Pregla, "Analysis of nonlinear properties of fibre grating structures", *Intern. J. Electron. Commun. (AEÜ)*, vol. **53**, pp. 25-31 (1999).

17. R. E. Collin, "*Field Theory of Guided Waves*", 2nd ed., IEEE Press, 1991, p. 419.

18. R. Pregla, "The method of lines for analysis of dielectric waveguide bends", *J. Lightwave Technol.*, vol. **14**, pp. 634-639 (1996).

19. K. A. Winick, "Effective-index method and coupled-mode theory for almost-periodic waveguide gratings: a comparison", *Appl. Opt.*, vol. **31**, no. 6, pp. 757-764 (1992).

20. S. Helfert, R. Pregla, "Efficient analysis of periodic structures", *J. Lightwave Technol.*, vol. **16**, pp. 1694-1702 (1998).

Figure captions:

Figure 1: Schematic of refractive index variation (a) and apodisation profiles used in this paper; (a) square profile (unapodised), (b) triangular profile and (c) diamond profile.

Figure 2: Reflectivity convergence (in %) of MoL method for apodised fibre gratings with N = 2048 (curve 1) and N = 4096 (curve 2).

Figure 3: Reflectivity functions of unapodized (curve 2) and apodized (1,3) fibre gratings with $N = 4096$. Curve 1 states for complete and curve 3 for partial decreasing core index step.

Figure 4: Electric field modulus (a) and and phase (b) distribution as a function of the normalised fibre radius of the forward- and backward-propagating fields for wavelengths corresponding maximum (λ_1), 3dB (λ_2) and minimum (λ_3) reflectivity.

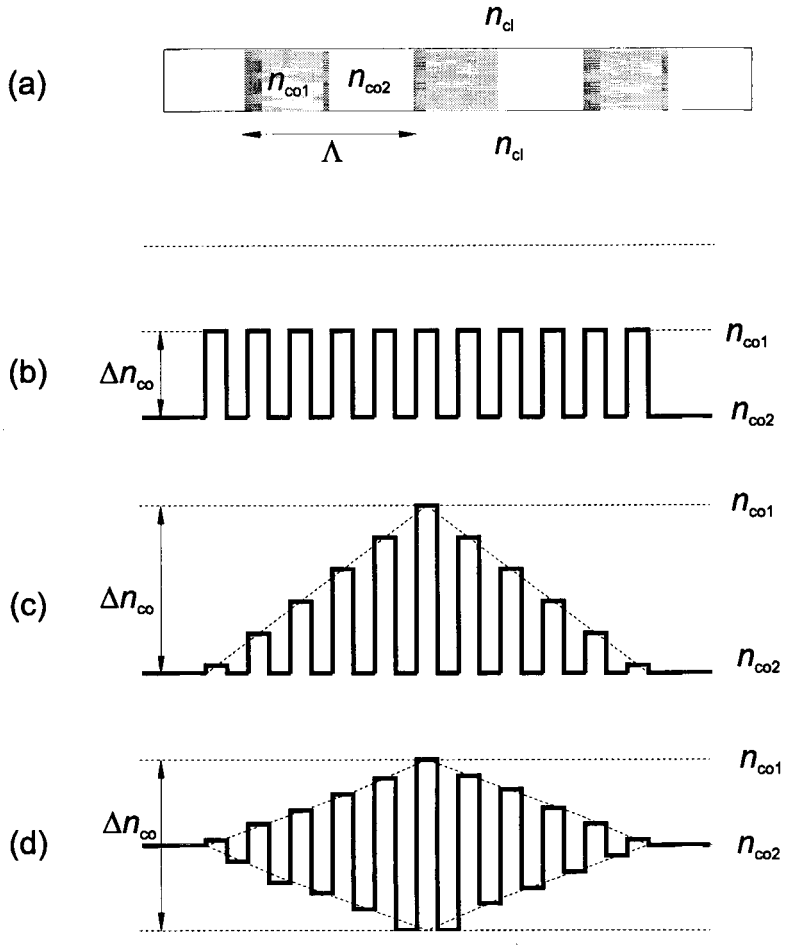

Figure 1: Schematic of refractive index variation (a) and apodisation profiles used in this paper; (a) square profile (unapodised), (b) triangular profile and (c) diamond profile.

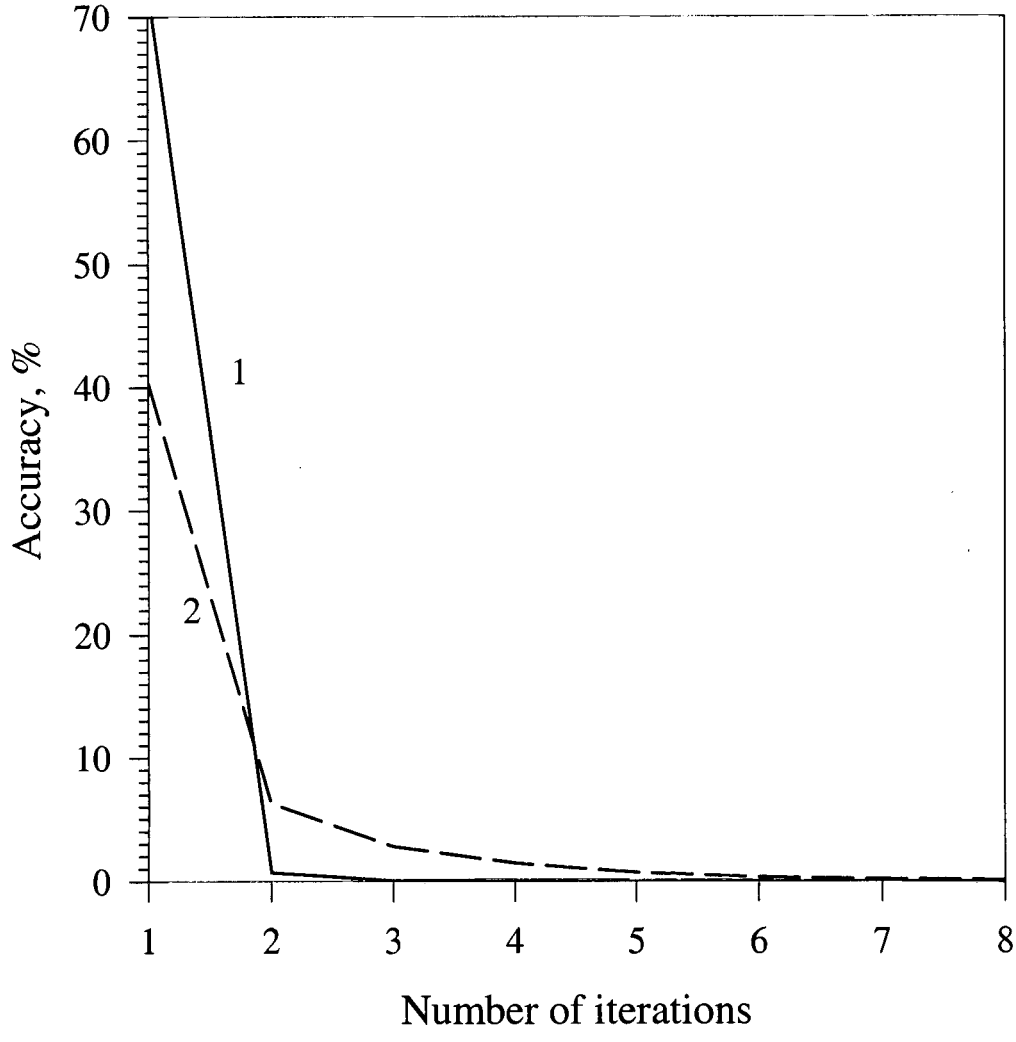

Figure 2: Reflectivity convergence (in %) of MoL method for apodised fibre gratings with N = 2048 (curve 1) and N = 4096 (curve 2).

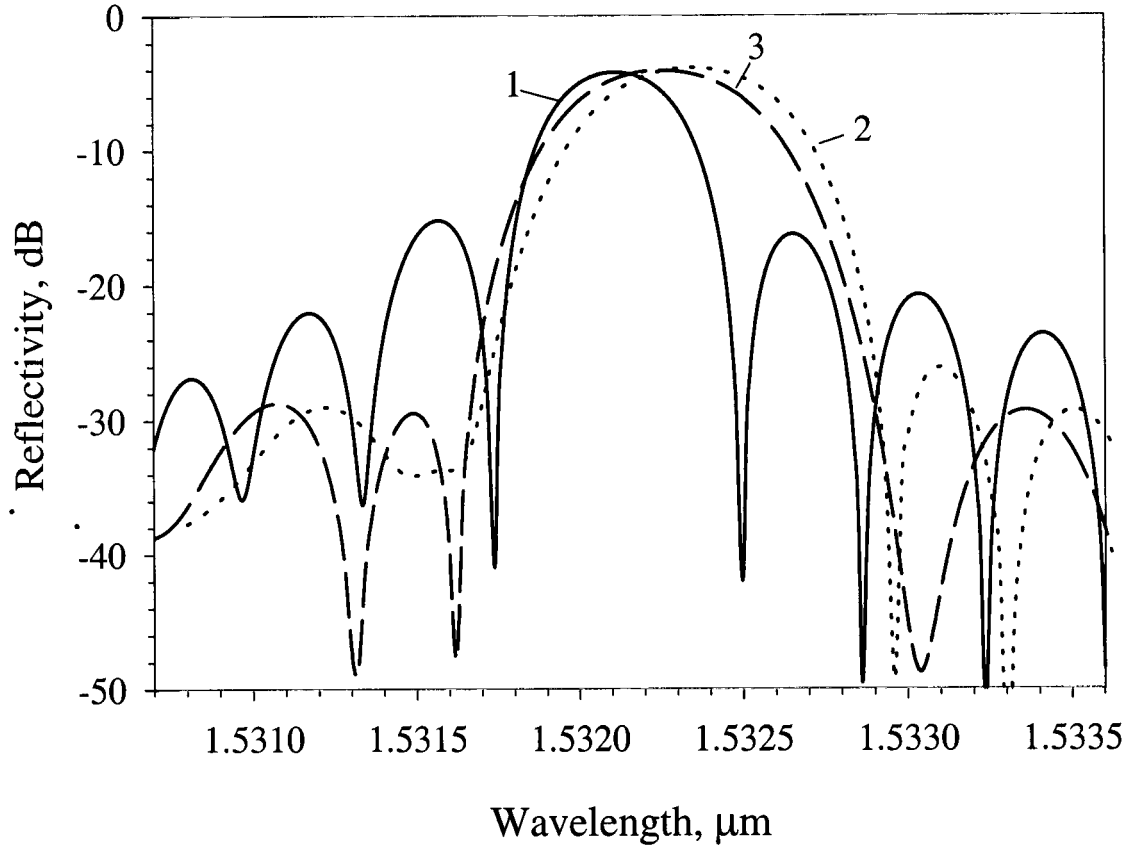

Figure 3: Reflectivity functions of unapodized (curve 2) and apodized (1,3) fibre gratings with $N = 4096$. Curve 1 states for complete and curve 3 for partial decreasing core index step.

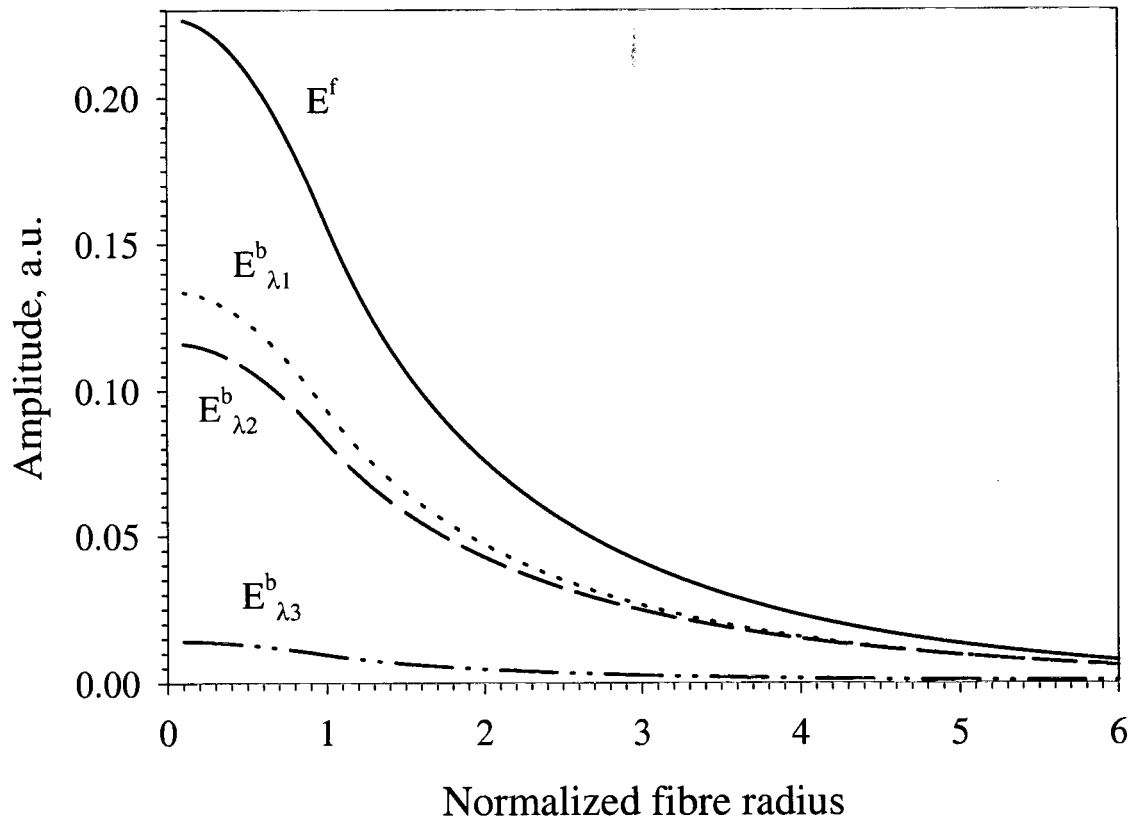
Amplitude, a.u.
0.20
0.15
0.10
0.05
0.00
E^f
$E^b_{\lambda 1}$
$E^b_{\lambda 2}$
$E^b_{\lambda 3}$
0
1
2
3
4
5
6
Normalized fibre radius

Figure 4a.

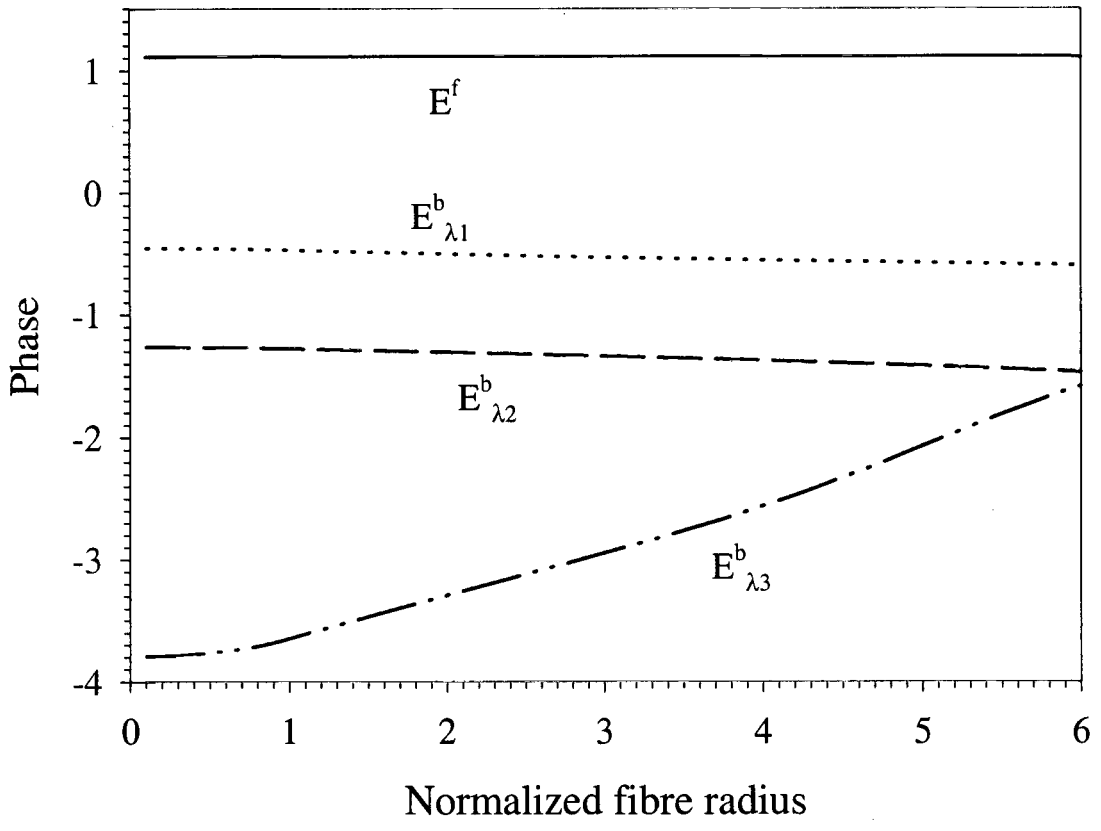

Figure 4b.

Figure 4: Electric field modulus (a) and and phase (b) distribution as a function of the normalised fibre radius of the forward- and backward-propagating fields for wavelengths corresponding maximum (λ_1), 3dB (λ_2) and minimum (λ_3) reflectivity.